A Computational Insight to Evaluate Performance of Fluorescein Dye, 7-Diethylamino-4-Methylcoumarin

Majid Ali[1*], Muhammad Sikandar Subhani[1], Farhat Ibraheem[1], Muhammad Suleman[1], Freeha Hafeez[1], Komal Sana[1]
[1]Department of Chemistry, Faculty of Engineering and Applied Sciences, Riphah International University Faisalabad, Faisalabad, Pakistan

ABSTRACT

The study under consideration represented the computational calculations of spectroscopic analysis of selected fluorescein dye named 7-Diethylamino-4-methylcoumarin (DEMC). Molecular Orbital (MO) calculations and the quantum mechanical calculations were studied in computational calculations. The MO calculations were done by using Hyper Chem program with semi-empirical AM1 and PM3 approximations. Quantum mechanical calculations were done by using Gaussian 09W. UV-Visible emission and absorption spectra included the relative energies ionization potential, infrared spectrum, and UV-Visible spectra. Calculations of solvents of low to high relative permittivity using molecular orbitals methods were studied for absorption spectra. The computed geometry of fluorescein dye was compared with those found experimentally/MP2 in gas phase. Solvatochromic study was done to check the effects of hydrogen bonding for the solvents. All the calculated results were compared with the available experimental data. HOMO-LUMO energy and MESP studies were also carried out to find the energy gap in gas and different solvents. Detailed comparison of Dye was evaluated in solvents to find the properties of dye for its useful applications. Absorption spectra were observed at 351 nm for water and acetone at 338 nm. HOMO and LUMO energy gap found for gas phase, water and acetone was -6.9816, -2.4386, and -6.5726 respectively. Following the obtained results, it was observed that dye has good interaction with acetone for its fluorescent use.

Keywords: Molecular orbital, DFT, Gaussian 09W, Spectroscopic properties, Fluorescein dye

1. Introduction

Fluorescein dyes are non-ionic aromatic chemical compounds that can easily dissolve in biological solvents. These dyes are offered in various color sequences, including Green, Orange, Black, Blue, Red, Brown, and purple. The main components of these dyes are Fluorescein Dye, anthraquinone dyes, and 7-Diethylamino-4-methylcoumarin (DEMC). Fluorescein dyes and their derivatives have extensive applications in the dyestuff industry.

According to current knowledge, Fluorescein Dyes formed from pyridine-2,6-dione-based join processes primarily consist of bilateral enantiotropic isomers such as pyridine-2,6-dione and 2-hydroxy-6-pyridone (Jung et al., 2012). DEMC holds particular significance as a prominent compound in this category. Computational structural determination methods can ascertain properties related to the dihedral angles, bond length, angles, geometric conformation, between planes, and other features of molecules. These structural characterizations are valuable for understanding intramolecular and intermolecular interactions at the biomolecular level. However, in dye fixation, adhering and spreading, and printing is examples of industrial uses, etc., computational investigations are not typically used to explore conformational modifications caused by isomerization, tautomerism, or the stereochemistry of substances (Huang, 2008).

Fluorescein Dyes are synthetic dyes renowned for their excellent stability, versatility, and a broad spectrum of colors. They find applications in various domains and technologies, such as textile fibers, nonlinear optics (NLO), biological fields, chemosensors for coloring multiple materials, and optical stereo data storage. However, it is essential to be cautious about certain dyes containing chromophores that release carcinogenic amines upon reductive cleavage, posing potential environmental risks (Ziarani, Moradi, Lashgari, & Kruger, 2018). The production of Fluorescein Dye DEMC currently holds a prominent position in the field of dye chemistry, and its significance is likely to grow further in the future. These dyes play a critical part in regulating the printing and pigment markets. The manufacturing process involves a straightforward diazotization and coupling procedure (Wang et al., 2022). Various techniques and modifications are applied to achieve optimal dispersion to ensure the dye possesses the anticipated color characteristics, particle size, and yield. Remarkably, Fluorescein dyes account for over 60% of all stains, making them the predominant category among shades. Besides their adverse impacts on humans and natural life, the pigments have prompted crucial demands for their removal from wastewater or conversion into safe and beneficial products. Furthermore, the color dispersion in water increased as the molecular weight of Fluorescein Dye grew, and DEMC dyes increased due to the production of more Fluorescein Dye connections. This increase in the absorption of the dye in water was

probably driven by a slowing of the Fluorescein Pigment DEMC dye breakdown process (Benkhaya, M'rabet, & El Harfi, 2020).

The uses of fluorescein pigments are diverse and extend to fields such as optics and the study of stereo-tautomeric equilibrium. Employing a computational software program and compactness efficient concept, we aim to explore how solvents affect Fluorescein Dye DEMC. Computational approaches are highly valuable, especially when dealing with rare or prohibitively expensive materials. By investigating the chemical characteristics of DEMC through computational calculations, we can make informed predictions before conducting actual experiments, enhancing our preparatory phase. Quantum mechanical calculations, a subset of computational analysis, offer valuable insights into molecules' constancy, energetics, and reactivity (Huang, 2008).

2. Materials and Methods

2.1 Material

During our research, we opted for Fluorescein Dye, specifically DEMC, and investigated its spectroscopical and microelectronic characteristics in various diluents.

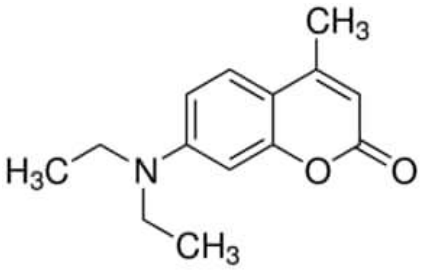

Figure 2.1: Structural formula of Fluorescein Dye DEMC

2.2 Gaussian and Hyperchem

The presented work used computational programs Gaussian 09W and Hyperchem to perform calculations. Gaussian is a contemporary electronic structure software commercially available under a US license. This program is a systematic and convenient multipurpose quantum chemistry instrument focusing on open-shell substances' spectroscopic features. Gaussian 09 can calculate various spectra, such as Raman Optical Activity (ROA), UV/Visible, IR, and Vibrational Circular Dichroism (VCD). Gauss View, a graphical user interface, is provided to simplify input preparation for Gaussian and visually inspect its output. Gauss View functions as a processor that works on both the front and back sides, streamlining the application of Gaussian instead of being directly integrated into its computational

module (Frisch, 2009). The software helped to customize sphere radii, stick dimensions, shading, and highlighting, making creating stereo and perception views effortlessly. Notably, Hyper Chem stands out from its competitors due to its powerful ability to visualize hydrogen bonding, a feature lacking in most other modeling tools (Laxmi & Priyadarshy, 2002).

2.3 Methodology

The selected compound was undergone complete geometry optimization using the DFT method using Gaussian 09W software with Becke's three-parameter composite exchange-correlation (B3LYP) functional. For this purpose, the basis set 6-31G(d) was used. The preference for 6-31G(d) for geometry improvements is likely due to its superior relative energies, despite being approximately five times lower than the 3-21G(d) origin (Geerlings, De Proft, & Langenaeker, 2003).

Additional graphical programs, such as ORIGIN, MOLDEN, and gOpenMol, played a crucial role in successfully conducting calculations on the data. Among these programs, MOLDEN was a software tool for pre-and post-processing data derived from computational chemistry programs. It facilitates interactions with packages like MOPAC, Games-US/UK, and Gaussian, focusing primarily on the computation and display of electronic and molecular properties. MOLDEN's capabilities also extend to simulating reaction pathways and other relevant aspects (Schaftenaar & Noordik, 2000).

Hyperchem conducted MO (molecular orbitals) calculations encompassing potentially energetic surfaces for quantum or conventional networks and particular points, geometry, and state of transition computations. It also integrates molecular dynamics and accounts for the impacts of thermal motion. The optimization's output provided crucial information such as the best molecule shape, entire molecular power, and moment of dipole attraction (Laxmi & Priyadarshy, 2002). The discussion topics included IR and UV-Visible. Geometry, spectral study, HOMO LUMO, MESP, and Mullikan analysis was done with DFT/B3LYP employing 6-31d basis set (Lewars, 2011).

2.3.1 Geometry optimization

The Polarizable Continuum Model (PCM) optimized the solution morphology. The objective was to calculate the excitation energies of the compound through TD-DFT

calculations, which has been performed based on optimized geometries for both gas and liquid (Barone, Cossi, & Tomasi, 1998). In order to calculate the absorption spectra, molecular orbital methods in solvents with varying relative permittivity, ranging from low to high was performed. The PM3/OSMO method was utilized to obtain all configurations. A comparison was made between the substance's predicted spectral shift operating a multi-electron arrangement interaction treatment and the experimental changes observed in both protic and aprotic media. Additionally, the overall alterations detected in different solvents were contrasted with the calculated shifts obtained through CNDO/S methods. This investigation aimed to determine the suitability for continuous solvation algorithms of non-protic liquids, such as polarization, while using a continuum model considering the inclusion of explicit solvent molecules to take into consideration the impact of hydrogen bonds in reactive solvents like water (Rana, Dhar, Sarkar, & Bhattacharya, 2011).

3. RESULTS AND DISCUSSION

3.1 Geometry parameters

Our research revolved around a theoretical investigation of the fluorescein dye compound, namely DEMC. This dye has a chemical formula of $C_{14}H_{17}NO_2$ and a molecular weight 231.29. By utilizing DFT with 6-31G(d) fundamental group and B3LYP, we computed the geometric properties of the dye in both gas and various solvent environments. We compared the results with experimental data/MP2 findings, which exhibited a remarkable agreement between them. From an optimized structure, the stability of a compound in a specific solvent was predicted. The optimization process for the dye involved different steps in gas and solvents such as water and acetone. The C1-C2 bond length was 1.3351 for gas, water, and acetone, while the C2-C3 bond length for acetone, water, and gas was 1.5307. Notably, the detected bond lengths remained consistent, and there is no evidence of a solvent influence on the structure of the title fluorescent pigment across the various mediums (Johnson & Becke, 2005).

Figure 3.1: Optimized structure of DEMC using the DFT/B3LYP/631G(d) modelling method

Table 3.1: An investigation to compare the computed bond lengths with the experimental bond lengths of Fluorescein Dye DEMC (Lawson & Pappas, 2023).

	Calculated bond length measurements			MP2
Parameters	**Acetone**	**Water**	**Gas**	**Gas**
C1-C2	1.3351	1.3351	1.3351	1.3351
C1-H18	2.05	2.05	2.05	2.05
C2-C3	1.5307	1.5307	1.5307	1.5307
C2-N7	2.45	2.45	2.45	2.45
C3-C4	2.3458	2.3458	2.3458	2.3458
C3-H19	2.05	2.05	2.05	2.05
C4-C5	1.5237	1.5237	1.5237	1.5237
C4-O11	1.4267	1.4267	1.4267	1.4267
C5-C6	2.3442	2.3442	2.3442	2.3442
C5-C8	1.5168	1.5168	1.5168	1.5168
C6-H20	2.05	2.05	2.05	2.05
C7-C14	1.46	1.46	1.46	1.46

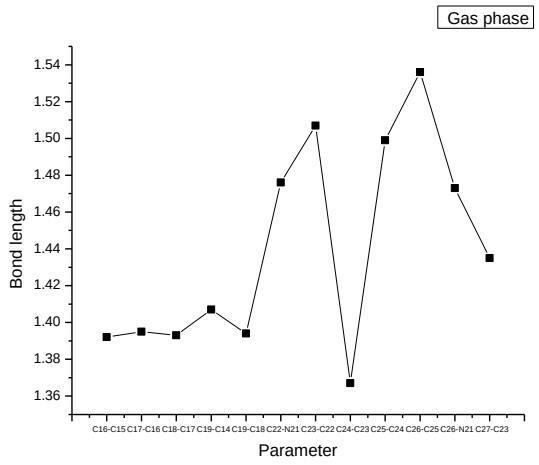

Figure 3.2: An assessment of the computed geometry

3.2 Mullikan Charges Analysis

The quantum mechanical calculation has been executed on a molecular scale, where the essential aspect involves Mullikan atomic charge calculations to explore the electron distribution of an entire molecule. These computations gave details about the substance's polarity and chemical reactivity, contributing to estimating its molecular structure (Carbó-Dorca & Bultinck, 2004). The Mulliken atomic charges were determined by applying the B3LYP algorithm and a 6-31G(d) basis set in Density Functional Theory (DFT). The results of these computations, which were carried out in both the gaseous state and several media, are shown in Table 3.2.

Table 3.2: Mullikan charge distribution, acquired through DFT/B3LYP calculations, under different solvent conditions, including gas phase.

Atom	Gas	Water	Acetone
1C	-0.214799	-0.2013	-0.229204
2C	0.330724	0.384797	0.322384
3C	-0.234743	-0.28588	-0.233968
4C	0.289668	0.309840	0.281603

5C	0.103305	0.074400	0.094797
6C	-0.242347	-0.22843	-0.249949
7N	-0.465749	-0.4997	-0.47815
8C	0.153828	0.198366	0.156623
9C	-0.269587	-0.32509	-0.281373
10C	0.599967	0.597597	0.610368
11O	-0.530245	-0.53546	-0.542853
12O	-0.473904	-0.55377	-0.524389
13C	-0.522896	-0.54099	-0.524526
14C	-0.149856	-0.15010	-0.153116
15C	-0.133362	-0.15561	-0.138877
16C	-0.471226	-0.45385	-0.476315
17C	-0.460758	-0.45219	-0.463638
18H	0.134756	0.155627	0.157824
19H	0.12229	0.15708	0.126416
20H	0.143317	0.158611	0.169334
21H	0.158786	0.154713	0.173217
22H	0.171229	0.184394	0.182424
23H	0.176804	0.177766	0.186368
24H	0.184759	0.184995	0.195534
25H	0.136357	0.166809	0.144759
26H	0.163434	0.165519	0.173699
27H	0.140493	0.165872	0.147727
28H	0.158565	0.167336	0.169474
29H	0.151577	0.156437	0.158135
30H	0.158878	0.16237	0.165833
31H	0.165108	0.159436	0.161667
32H	0.214390	0.160343	0.218806
33H	0.143219	0.156657	0.148417
34H	0.167786	0.161386	0.163076

The impact of solvents on atomic charge distribution was investigated through Mulliken analysis of the biological population and DEMC pigment. This analysis used multiple basis sets and solvents at the B3LYP level. Mulliken atomic charge calculations performed a crucial part in quantum biological studies of fragments as they enable the computation of various molecular properties, including electronic structure and dipole moment, among others (Wahab, Olasunkanmi, Govender, & Govender, 2018a).

Each hydrogen atom contains concentrated positive charges. These positive charges are inherent to each hydrogen atom. The maximum negative charge value were observed within all environments for O12 was approximately -0.553779. A similar pattern was noticed for 10C, outlining regions of the highest electron density around the oxygen atoms in the studied dye. The diverse polarities of the solvents led to minor fluctuations in the distribution of atomic charges across different solvents (Wahab, Olasunkanmi, Govender, & Govender, 2018b).

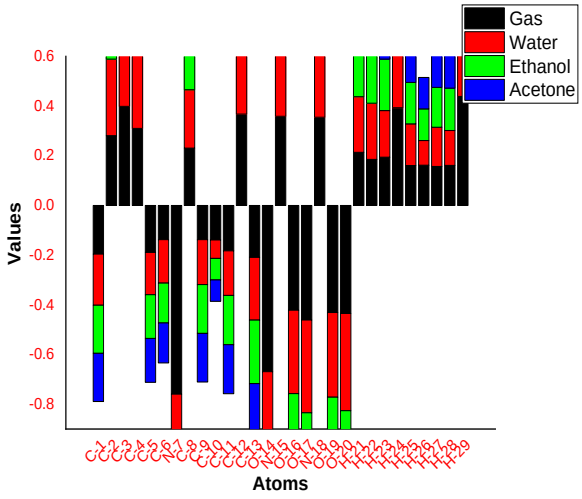

Figure 3.3: Mulliken atomic charge values in a gaseous state and various solvent environments

3.3 Electronic Absorption Spectral Study

When a continuous illumination source stimulates molecules to emit light, the subsequent photons or brightness levels are observed while varying the wavelength. This process generates consistent fluorescence spectra. In cases where the wavelength used for stimulation remains constant, and the emitted wavelength is analyzed to create a graph illustrating the relationship between brightness and emitted wavelength, the outcome is referred to as a fluorescence emission spectrum. In contrast to an absorbance spectrum that encompasses all absorbing entities within a substance or material, excitation spectra focus solely on emitting wavelength. The emission and excitation spectra exhibited a symmetrical relationship for a specific fluorophore (Sciortino, Marechal, Fabian, Lihi, & Garribba, 2020).

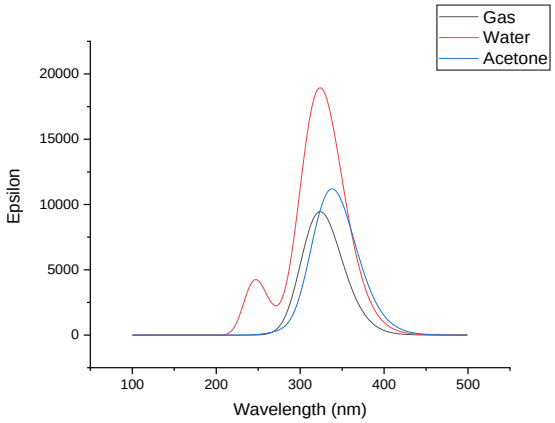

Figure 3.4: DEMC's UV-visible spectrum in different solutions

Table 3.3: DEMC electronic transition coefficients

Phase	Transition with Contribution	Wavelength (nm)	Oscillator strength(f)
Gas	Excited states 1 H → L (67%)	323	0.2307
	Excited states 2 H-3 → L (40.08%)	296	0.0064
	Excited states 3 H – 5 → L (13.24%) H – 1 → L (66.97%)	269.7	0.0003
Water	Excited states 1 H → L (71.39%)	350	0.0734
	Excited states 2 H → L + 1 (71.11%)	286	0.4552

	Excited states 3 H – 5 → L (1195%) H – 1 → L (67.98%)	265	0.0412
Acetone	Excited states 1 H → L (71.03%)	337	0.0756
	Excited states 2 H → L + 1 (71.11%)	291	0.0059
	Excited states 3 H – 5 → L (14.99%) H – 1 → L (68.01%)	272	0.0028

The Fluorescein DEMC dye's UV-Vis spectra were computed for gaseous and various solvent media (including acetone and water). While the absorption peak remains relatively stable across different solvents, a notable difference arises in the gas phase, where the most negligible absorption occurs at 323 nm. Comparing the visible and UV regions, the latter display considerably higher absorption. The TD-DFT research used in the surroundings of the first excited state reveals a red shift from gas to water, with a notably more pronounced change observed within solvents than gases. Within a solution, a relationship between solute and solvent components significantly influences the molecule's shape and electronic structure, thus enabling the acquisition of UV-visible spectra in a dissolved state (Deshmukh & Sekar, 2014). Table 3.3 summarizes the TD-DFT computations to describe the absorption spectrum traits of the Fluorescein Dye DEMC. The absorption spectrum exhibited at 350 nm in the case of water and at 337 nm in acetone. A noticeable blue shift was noted during the transition from water to acetone, indicating the favorable interaction of the DEMC dye with acetone for its fluorescent application (Jacquemin, Perpète, Ciofini, & Adamo, 2010).

3.4 Frontier molecular orbitals (HOMO-LUMO)

The computation involved determining the energy levels of DEMC dye's HOMO-LUMO orbitals in gaseous form and solvents and displaying the optimized dispersion yellow 01 material's electrical traits employed Gauss View 5.0. This paper presents the outcomes, while figures 3.5–3.7 provide orbital visualizations of HOMO and LUMO frequencies (Mumit et al., 2020). The HOMO and LUMO in the gas phase, water, and acetone energy gap values were found to be -6.9816, -2.4386, and -6.5726, respectively. These energy gap measurements offer insights into the planarity and polarity of the dye. A smaller energy gap was noted in acetone, indicating that DEMC possesses lower chemical rigidity

and planarity within acetone. It Suggested that DEMC could yield favorable outcomes when utilized with acetone in applications such as fluorescein and textile treatment. Researching the HOMO-LUMO energies also helped to understand chemical toughness, which influences a substance's durability. Wide HOMO-LUMO energy disparities indicate flexible particles, whereas small HOMO-LUMO potential gaps indicate complex molecules typify more rigid compounds (Odey et al., 2021).

The table displayed various chemical activity parameters. This situation exhibits greater reactivity and sensitivity in a diverse interaction environment, enabling it to alter its electrical structure and properties. For significant electron delocalization to take place, compounds need to possess poor electronegativity, poor chemical hardness, and significant chemical susceptibility (AĞirtaŞ, SolĞun, Yildiko, & Özkartal, 2020).

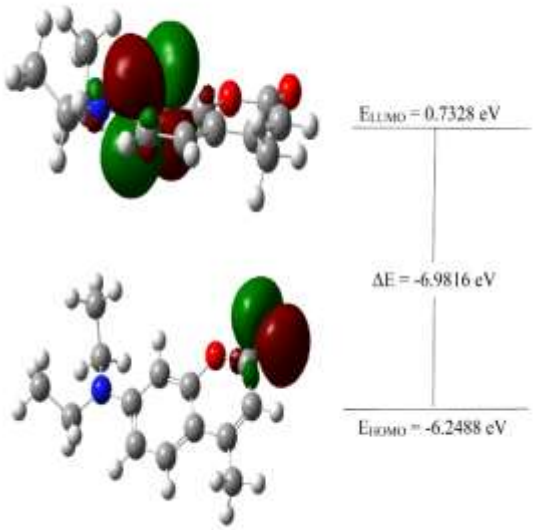

Figure 3.5: The Energy gap of DEMC in Gas

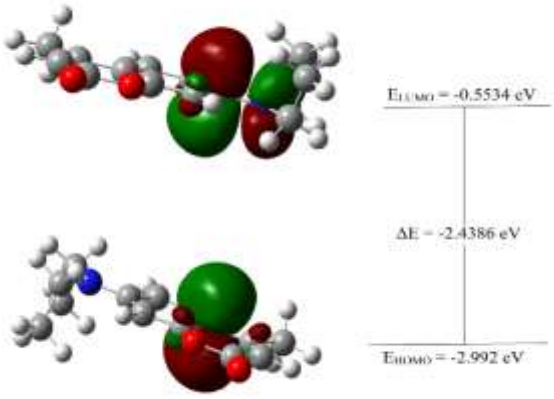

Figure 3.6: The Energy gap of DEMC in water

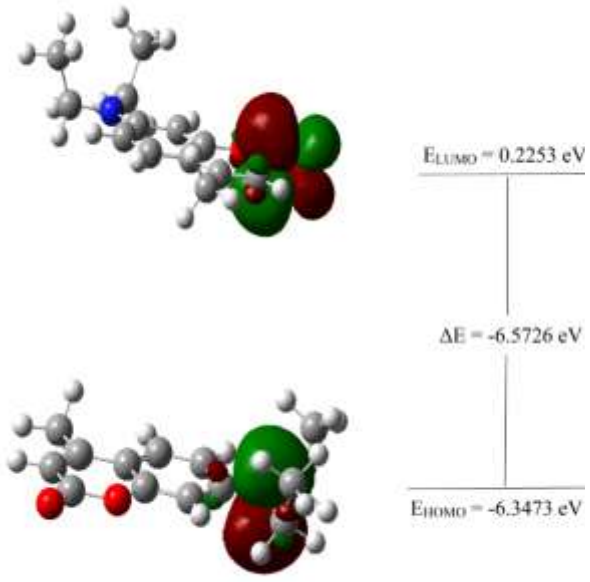

Figure 3.7: The Energy gap of DEMC in acetone

3.5 Spectral Analysis of Vibrations

The compound under observation belongs to the C1 point group. In descending sequence, the estimated fundamental vibrational frequency patterns are displayed. The numerous vibrational methods ascribed to the detected Bands of FT-IR and FT-Raman are documented in Table 3.4. Predicted vibrational frequencies for Fluorescein Dye DEMC are depicted in Figure 3.8 in gas and various solvents (water or acetone), scaled by a factor of 0.96. This figure also encompasses the pigment compounds determined by FT-IR spectra (Merrick, Moran, & Radom, 2007).

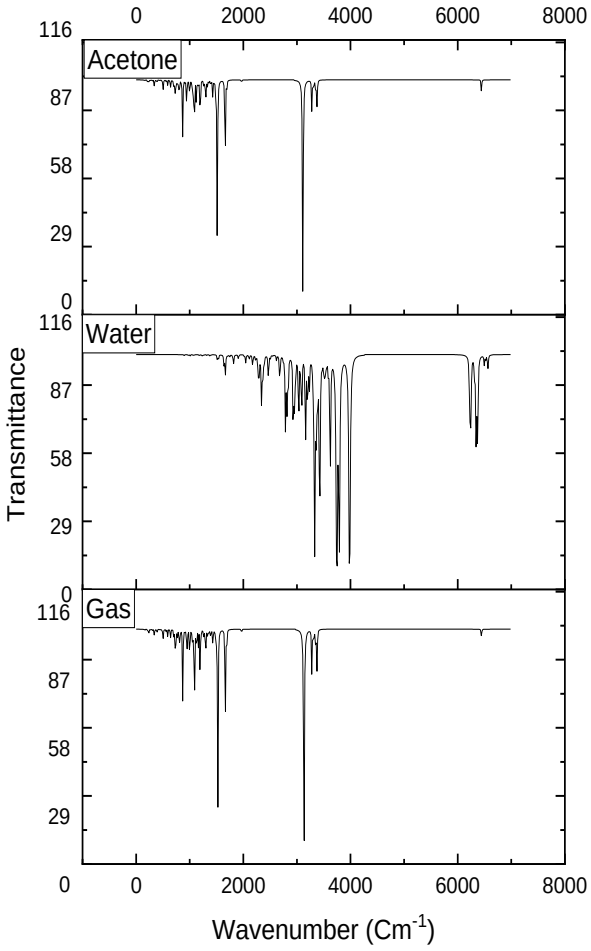

Figure 3.8: Display of IR spectra for Fluorescein Pigment DEMC carried out in the gaseous phase and various solvent environments

Table 3.4: Vibrational spectra of DEMC computed in both the gas phase and several solvents

PED Project (≥10 percent)	Designed wavenumber (cm^{-1})		
	Gas	Water	Acetone
$\mathcal{V}$CHasym (-67)	3380.85	3252.23	3379.72

$\mathcal{V}$CHsym (81)	3373.47	3225.13	3374.60
$\mathcal{V}$CHaym (-11)-$\mathcal{V}$CHasym (-75)	3372.34	3210.51	3372.58
$\mathcal{V}$CCsym (69)	1692.24	1776.72	1690.76
$\mathcal{V}$OCsym (84)	1526.43	1571.26	1517.28
βHCHsym (64)-Tors HCCNsym (12)	1518.36	1567.2	1511.15
βHCHsym (12)-βHCHsym (60)	1506.47	1550	1499.1
βHCHasym (-66)-Tors HCCCsym	1471.70	1512.77	1459.59
$\mathcal{V}$CCsym (49)-βHCHsym (24)	1433.53	1507.56	1429
βHCCasym (-27)-Tors HCNCsym (26)	1389.55	1497.59	1390.30
Tors HCNCasym (-34)-Tors	1379.83	1488.86	1378.60
$\mathcal{V}$OCsym (14)-βCOCasym (-12)	1124.93	1257.71	1121.01
$\mathcal{V}$CCsym (12)-Tors HCCNCsym (13)	1095.8	1234.93	1091.25
$\mathcal{V}$CCsym (14)-Tors CNCCsym (14)	1079.96	1198.46	1078.28
$\mathcal{V}$NCsym (21)-$\mathcal{V}$CCsym (16)	1072.37	1185.01	1071.7
βHCHsym (66)-Tors HCCCsym	1015.83	1120.26	1014.10
$\mathcal{V}$CCsym (17)-$\mathcal{V}$CCsym (12)	1006.94	1109.86	1004.77
Tors HCCCsym (26)	995.85	1095.95	993.70

Tors HCCCasym (-12)	760.08	848.7	756.99
Tors HCCCsym (38)-Out NCCCasym	646.85	741.66	648.96

3.6 Fluorescein Dye 7-Diethylamino-4-methylcoumarin(DEMC)

Every IR-active vibration corresponds to a normal mode of motion. The assignment of these vibrations involves assessing their intensity and line shape, a task facilitated by the VEDA 4 program. Additionally, GaussView 5.0 software was employed to create animations for visualization. The initial three vibrations primarily involved symmetric stretching and fall within the approximate range of 3000 cm^{-1}. The content of 3300 cm^{-1} displayed the CH antisymmetric vibrations, while the region around 3200 cm^{-1} exhibits the C-H in-plane bending vibration.

Additionally, CH torsion vibrations around 1000 cm^{-1} have been identified. Various frequency bands in Table 3.5 depicted related vibrations In-plane bending and twisting of HCC Vibrations of HCCC. The symmetric vibrations of Out OCOC fall within the 1100-1200 cm^{-1} range across all media. Typically, bands displaying different intensity levels can be seen within the 500-3300 cm^{-1} range, according to the frequency details outlined in Table 3.4. Vibrations related to H-C-H bonds occured between 1000-1500 cm^{-1}. Vibrational frequency values varied between gas and solvent systems, indicating the influence of the solvent on the results.

3.7 Molecular Electrostatic Potential

The molecule's electrical charge distribution can be acquired using a map of its electrophilic potential (MEP). The significance of the electron distribution density in the molecule becomes evident by describing bonds polarity and electronegativity of compound. The intricate electron configuration of complex molecules and the spatial attributes of molecular reactions can be complicated. MEP patterns are visualized through the Gauss View 05 programmed and the DFT/B3LYP/6-31G(d) scale of theory (Mumit et al., 2020). Analysis of the MEP diagram demonstrated that the zone surrounding the Fluorescein Pigment DEMC showed positive values, as indicated by the blue shade. Regions highlighted in red on the map signify areas with a high electron density. The more significant part of the heterocyclic area displays an almost neutral potential, depicted by a hue that is a blend of yellow and green.

In contrast, the nitro core shows decreased stability with a blue color, while the core structures of the Fluorescein Dye DEMC exhibit a distributed arrangement and significant stabilization, represented by hues leaning towards green and yellow (Suresh, Remya, & Anjalikrishna, 2022).

The analysis yielded electrophilic potential (MEP) maps for DEMC molecules. These maps were visualized using Gauss View 05 software at the level DFT/B3LYP/6-311Gd, as shown in Figures 3.9 and 3.10. The MEP maps highlight distinct features: the region surrounding the Oxygen atoms is represented in red, indicating elevated electron density. Conversely, the aromatic and nitro ring areas display predominantly neutral potential, characterized by a yellow-green shade. Notably, the Fluorescein Dye DEMC's core structures exhibit a delocalized configuration and significant stability, as evident from the green-yellow hues present (Numbury, 2022).

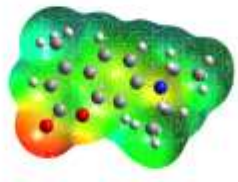

Figure 3.9: The solid-phase MESP of DEMC dye

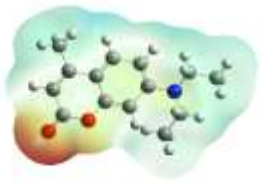

Figure 3.10: DEMC dye Mesh structure

4. Conclusion

The ongoing research employed the Fluorescein Dye DEMC, known as 7-Diethylamino-4methylcoumarin (DEMC), as the subject of quantum mechanical computations. These computations were facilitated by using computational apparatus. The basic program utilized in this research encompasses Hyperchem 8.0 and Gaussian 09W, while supplementary tools like Gauss View 5.0, Avogadro, MS Excel, Moltran, VEDA 4, and Origin were also integrated. The manipulation and handling of data related to the dye compound were executed by applying computational techniques such as Ab-Initio, Semi-Empirical, Hartree-Fock (HF), and Density Functional Theory (DFT). This comprehensive computational analysis delved into diverse parameters and their characteristics, including geometric aspects, energetics, distribution of atomic charges, solvent impacts, natural bonding orbitals, and spectroscopic evaluation. The dry lab calculations performed for dye in various environments using DFT with the B3LYP,

and the 6-31G(d) demonstrated, dye can better perform in acetone for its fluorescent use.

REFERENCES

AĞirtaŞ, M. S., SolĞun, D. G., Yildiko, Ü., & Özkartal, A. (2020). Design of novel substituted phthalocyanines; synthesis and fluorescence, DFT, photovoltaic properties. *Turkish journal of chemistry*, *44*(6), 1574-1586.

Barone, V., Cossi, M., & Tomasi, J. (1998). Geometry optimization of molecular structures in solution by the polarizable continuum model. *Journal of computational chemistry*, *19*(4), 404-417.

Benkhaya, S., M'rabet, S., & El Harfi, A. (2020). Classifications, properties, recent synthesis and applications of azo dyes. *Heliyon*, *6*(1), e03271.

Carbó-Dorca, R., & Bultinck, P. (2004). The quantum mechanical basis for Mulliken population analysis. *Journal of mathematical chemistry*, *36*(3), 231-239.

Deshmukh, M. S., & Sekar, N. (2014). A combined experimental and TD-DFT investigation of three dispersed azo dyes having the nitroterephthalate skeleton. *Dyes and Pigments*, *103*, 25-33.

Frisch, A. (2009). gaussian 09W Reference. *Wallingford, USA*, *25p*, *470*.

Geerlings, P., De Proft, F., & Langenaeker, W. (2003). Conceptual density functional theory. *Chemical reviews*, *103*(5), 1793-1874.

Huang, W. (2008). Structural and computational studies of azo dyes in the hydrazone form having the same pyridine-2, 6-dione component (II): CI Disperse Yellow 119 and CI Disperse Yellow 211. *Dyes and Pigments*, *79*(1), 69-75.

Jacquemin, D., Perpète, E. A., Ciofini, I., & Adamo, C. (2010). Assessment of functionals for TD-DFT calculations of singlet-triplet transitions. *Journal of chemical theory and computation*, *6*(5), 1532-1537.

Johnson, E. R., & Becke, A. D. (2005). A post-Hartree–Fock model of intermolecular interactions. *The Journal of chemical physics*, *123*(2).

Jung, H., Seok, S. H., Han, J. H., Abdelkader, T. S., Kim, T. H., Chang, S. N., . . . Seo, J. E. (2012). Effect of fluorescent whitening agent on the transcription of cell damage-related genes in zebrafish embryos. *Journal of Applied Toxicology*, *32*(9), 654-661.

Lawson, D. B., & Pappas, J. (2023). MP2 study of the adsorption of CO2 onto the water monomer, dimer and trimer. *Theoretical Chemistry Accounts*, *142*(1), 8.

Laxmi, D., & Priyadarshy, S. (2002). HyperChem 6.03. *Biotech Software & Internet Report: The Computer Software Journal for Scientists*, *3*(1), 5-9.

Lewars, E. (2011). Computational chemistry. *Introduction to the theory and applications of molecular and quantum mechanics*, 318.

Merrick, J. P., Moran, D., & Radom, L. (2007). An evaluation of harmonic vibrational frequency scale factors. *The Journal of Physical Chemistry A*, *111*(45), 11683-11700.

Mumit, M. A., Pal, T. K., Alam, M. A., Islam, M. A.-A.-A.-A., Paul, S., & Sheikh, M. C. (2020). DFT studies on vibrational and electronic spectra, HOMO–LUMO, MEP, HOMA, NBO and molecular docking analysis of benzyl-3-N-(2, 4, 5-

trimethoxyphenylmethylene) hydrazinecarbodithioate. *Journal of molecular structure*, *1220*, 128715.

Numbury, S. B. (2022). Designing of small organic non-fullerene (NFAs) acceptor molecules with an A− D− A framework for high-performance organic solar cells: A DFT and TD-DFT method. *Oxford Open Materials Science*, *2*(1), itac002.

Odey, J. O., Louis, H., Agwupuye, J. A., Moshood, Y. L., Bisong, E. A., & Brown, O. I. (2021). Experimental and theoretical studies of the electrochemical properties of mono azo dyes derived from 2-nitroso-1-naphthol, 1-nitroso-2-naphthol, and CI disperse yellow 56 commercial dye in dye-sensitized solar cells. *Journal of Molecular Structure*, *1241*, 130615.

Rana, D. K., Dhar, S., Sarkar, A., & Bhattacharya, S. C. (2011). Dual intramolecular hydrogen bond as a switch for inducing ground and excited state intramolecular double proton transfer in doxorubicin: an excitation wavelength dependence study. *The Journal of Physical Chemistry A*, *115*(33), 9169-9179.

Schaftenaar, G., & Noordik, J. H. (2000). Molden: a pre-and post-processing program for molecular and electronic structures. *Journal of computer-aided molecular design*, *14*(2), 123-134.

Sciortino, G., Marechal, J.-D., Fabian, I., Lihi, N., & Garribba, E. (2020). Quantitative prediction of electronic absorption spectra of copper (II)–bioligand systems: Validation and applications. *Journal of Inorganic Biochemistry*, *204*, 110953.

Suresh, C. H., Remya, G. S., & Anjalikrishna, P. K. (2022). Molecular electrostatic potential analysis: A powerful tool to interpret and predict chemical reactivity. *Wiley Interdisciplinary Reviews: Computational Molecular Science*, *12*(5), e1601.

Wahab, O. O., Olasunkanmi, L. O., Govender, K. K., & Govender, P. P. (2018a). A DFT study of disperse yellow 119 degradation mechanism by hydroxyl radical attack. *ChemistrySelect*, *3*(46), 12988-12997.

Wahab, O. O., Olasunkanmi, L. O., Govender, K. K., & Govender, P. P. (2018b). Synergistic effect of opposite polar substituents on selected properties of disperse yellow 119 dye. *Chemical Physics Letters*, *704*, 55-61.

Wang, M., Zhao, M., Liu, P., Zhu, H., Liu, B., Hu, P., & Niu, X. (2022). Coupling diazotization with oxidase-mimetic catalysis to realize dual-mode double-ratiometric colourimetric and electrochemical sensing of nitrite. *Sensors and Actuators B: Chemical*, *355*, 131308.

Ziarani, G., Moradi, R., Lashgari, N., & Kruger, H. G. (2018). *Metal-free synthetic organic dyes*: Elsevier.

Authors:

First Author – Dr. Majid Ali, PHD Chemistry, Assistant professor, Department of Chemistry Riphah International University, Faisalabad.

Second Author – Muhammad Sikandar Subhani, Bachelor of science in chemistry, Riphah International University, Faisalabad, .

Third Author – Dr. Farhat Ibraheem, PHD Chemistry, Riphah International University, faisalabad.

Fourth Author– Dr. Muhammad Suleman, PhD Chemistry, Riphah International University, faisalabad, .

Fifth Author – Dr. Freeha Hafeez, PhD Chemistry, Riphah International University, faisalabad
Sixth Author – Ms. Komal Sana, Riphah International University, Faisalabad

Correspondence Author – Dr. Majid Ali, PHD Chemistry, Assistant professor, Department of Chemistry, Riphah International University, Faisalabad.